Proceedings of the ASME 2017 36th International Conference on Ocean, Offshore and Arctic Engineering
OMAE 2017
June 25-30, 2017, Trondheim, Norway

OMAE2017-62548

WAVE-CURRENT INTERACTION EFFECTS ON AIRGAP CALCULATIONS

Elin Marita Hermundstad
SINTEF Ocean*
Trondheim, Norway

Jan Roger Hoff
SINTEF Ocean
Trondheim, Norway

Nuno Fonseca
SINTEF Ocean
Trondheim, Norway

Rune Bjørkli
Statoil
Stavanger, Norway

ABSTRACT

The importance of wave-current interaction effects on the determination of mean drift forces on floating offshore structures is well documented. Wave-current interaction effects will also influence the first-order motions and loads as well as the diffracted and radiated waves around the structure. One of the significant contributions to the influence of wave-current interaction effects on the motion responses is the additional coupling between motion modes due to the current. These effects are well known from seakeeping calculations of ships with forward speed. A structure with fore-aft symmetry will have no hydrodynamic coupling between heave and pitch in regular waves only. Due to the presence of a current, the symmetry of the flow around the body is lost, resulting in hydrodynamic coupling between the modes. This will also occur for a moored structure with slowly varying motions in the horizontal plane. The most important couplings are from the heave motion into pitch and surge and from heave to roll and sway. These couplings are otherwise present only for asymmetric structures. Due to the presence of the heave resonance and cancellation periods, the motion responses in roll and pitch for a semi-submersible will be influenced by the wave-current interaction effects. Due to the differences in phase between the different motion modes, the hydrodynamic coupling may have significant influence on the rotational motions roll and pitch and thus significant influence on the prediction of airgap. This coupling between the heave and roll/pitch modes due to the current adds complexity to the numerical simulations since the structure responses are more sensitive to the actual orientation of the structure, mooring configuration etc.

A three-dimensional linear potential flow code, MULDIF, has been developed by SINTEF Ocean. This code accounts for hydrodynamic interaction between waves and current from arbitrary directions. The code can be applied to single or multiple bodies in infinite or finite water depth. Verification studies have previously shown good agreement with other numerical codes, Hermundstad et.al. [1], Zhiyuan et.al [2].

Validation studies with emphasis on airgap and comparison with experimental results are presented and numerical results for airgap and upwell are visualized and discussed. It is demonstrated how MULDIF can be used in airgap studies.

INTRODUCTION

Semi-submersible platforms have found wide-spread use in the offshore industrial field. A key factor in the design of these is the airgap requirement. Sufficient deck clearance must be ensured to avoid damage from wave impacts to the deck superstructure. Accurate predictions of air gap is more complicated for floating structures as the platform is free to move in all six degrees of freedom. Further, large production semi-submersibles

*Earlier MARINTEK, SINTEF Ocean from 1st January 2017 through a merger internally in the SINTEF Group

are generally required to remain on location throughout the most severe weather conditions.

Numerical hydrodynamic diffraction analysis and model tests are commonly used to study wave-structure interaction as part of the design process. For large volume structures, the airgap prediction is complicated significantly by diffraction and radiation effects. Ignoring the diffraction effects will give non-conservative estimates of the airgap. Wave-current interaction effects will further influence the prediction of airgap in several ways and complicate the prediction even more. Firstly, wave-current interaction effects will influence the diffraction problem and change the diffracted wave field around the structure, Zhang et.al. [3]. Secondly, the wave-current interaction will influence the vertical motion response at a given location on the body. This is caused by current induced coupling terms in the added mass and damping matrices, Hermundstad et.al. [1].

The wave-current interaction has been found to be important for prediction of mean drift forces, Zhao et.al. [4]. It was found that waves and current propagating in the same direction was found to increase the mean drift forces. Collinear waves and current are also most commonly used in experimental studies of wave-current interaction effects. This may not necessarily result in the most severe conditions for airgap studies. Observations have for example shown impact occurring with a relative difference in direction between waves and current of 20-30 degrees at the time of impact, which relative to the body means a wave heading of 10-20 degrees and current direction 40 degrees.

Manuel et.al. [5] found that the wave elevation at field points close to the center of the platform exhibited the greatest non-Gaussian character relative to field points near a column. Further, it was concluded that the non-Gaussian character was largely a result of second-order diffracted waves.

A three-dimensional linear potential flow code, MULDIF, has been developed by SINTEF Ocean. This code accounts for hydrodynamic interaction between waves and current from arbitrary directions. The code can be applied to single or multiple bodies in infinite or finite water depth. Verification studies have previously shown good agreement with other numerical codes, Hermundstad et.al. [1], Zhiyuan et.al [2], with respect to predictions of motion responses and mean drift forces.

MOTION RESPONSES

In the design of floating offshore structures prediction of the wave elevation around the structure is important in order to design the structure with sufficient airgap to avoid large impact loads. Numerical studies have shown that wave-current interaction effects are important with respect to prediction of airgap, Zhang et.al. [3] and Bratland et.al. [9]. A consequence of the wave-current interaction is the coupling between heave and pitch (and heave-roll) due to the corresponding coupling terms in the added mass and damping coefficients. This is well known from

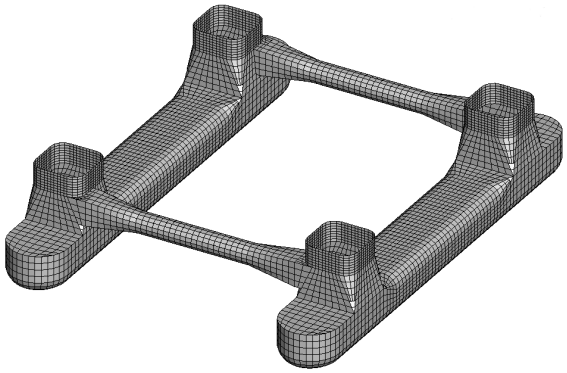

FIGURE 1. Panel model of the ExWave semi.

prediction of ship motions at forward speed where the forward speed effects on these coefficients are given explicitly from strip theory, Salvesen et.al. [10]. For an offshore structure which in general is symmetric about the longitudinal and transverse planes, the coupling coefficients without current or slowly varying motions are small. With current, the coupling from heave into roll and pitch may be important. The heave resonance will thus influence the roll and pitch motions.

Numerical calculations have been carried out for the ExWave semi-submersible, which is a generic model of a medium-sized drilling platform with two pontoons. It was tested in the Ocean Basin at SINTEF Ocean as part of the ExWave JIP, where the main purpose was to study drift forces in severe sea states. The panel models of the semi and the free surface are given in Figures 1 and 2, respectively. The free surface grid must be included to account for the interaction with the steady flow in the free surface condition when wave-current interaction effects are included. The numerical calculations include the effect of horizontal mooring and viscous effects in a simplified manner by introducing coupled surge-pitch restoring and drag forces on the pontoons and bracings. The calculations have been carried out for the survival draught loading condition.

Experimental results for the motions are available in the form of motion transfer functions obtained from cross-spectral analysis of test results in irregular sea states. The accuracy of the transfer functions depends on the level of energy present in both response and wave spectrum. Thus the obtained transfer functions are less accurate in the tale of the spectra.

Motion RAOs of the ExWave semi obtained from two sea states in head waves are shown in the Figures 3 to 8. Generally the agreement between the RAOs calculated by MULDIF and the measured RAOs is quite good.The RAOs obtained from the low sea state with significant wave height $H_s = 2.5$ m and pink noise are expected to give the best agreement with the calculated RAOs. The surge, heave and pitch motion RAOs with-

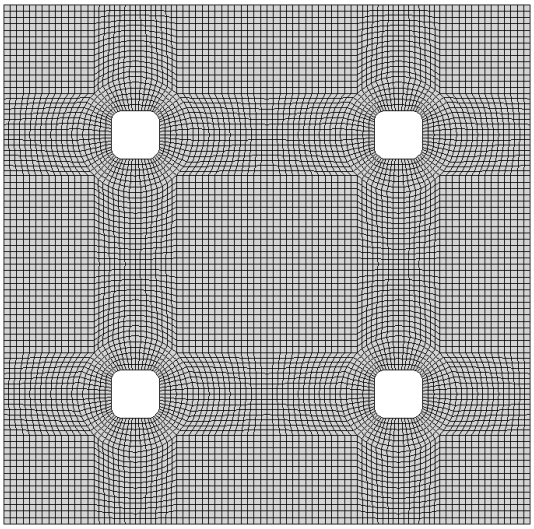

FIGURE 2. Free surface mesh of the ExWave semi.

out current are given in Figures 3, 4 and 5, respectively. The corresponding RAOs with current speed 0.9 m/s along the longitudinal axis are given in Figures 6, 7 and 8, respectively. The motion responses are plotted against the wave period for head waves. The RAOs obtained from the severe sea state ($H_s = 11.5$ m) are generally lower than the corresponding results obtained from the pink noise tests. This is due to nonlinear effects such as viscous forces. Additionally, contributions from the mooring system may explain the differences in the RAOs seen in the heave response around the cancellation period. This shows that contributions from mooring system and viscous forces are important in severe sea states and should be included in the numerical model.

In MULDIF the viscous forces are obtained by modeling the bracings and pontoons as drag elements, calculating the drag forces by a strip model using the drag term in the Morrison formula with drag coefficient $C_D = 1.2$. The quadratic terms of the viscous forces are then linearized using an equivalent linearization technique for each frequency applying a wave amplitude corresponding to the significant wave height. The resulting equations of motion are finally solved by iteration. The contribution from the mooring system is included as additional stiffness in the coupled surge-pitch mode. The coupled surge-pitch restoring coefficient is increased slightly for the more severe sea state to reflect the non-linearity in the mooring characteristics with mean offset. Tuning the additional stiffness to model the contribution from the mooring system is not straight forward due to the coupling between the modes of motion. In the presented results, focus has been on tuning the heave motion.

The slowly varying surge motion of the Exwave semi in the model tests may also have some influence on the measured RAOs because it will act like a time varying current speed. This again will influence the coupling between the modes of motion.

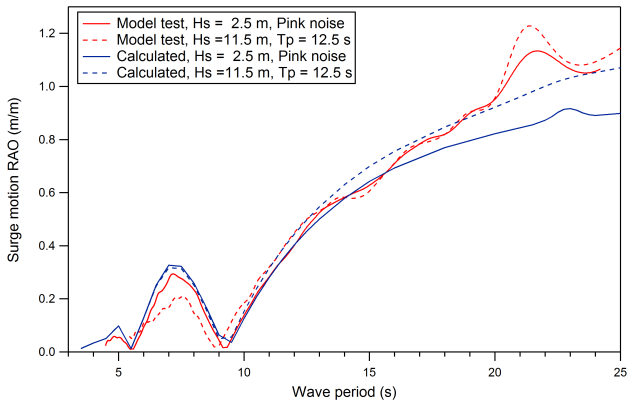

FIGURE 3. Surge motion response RAO without current.

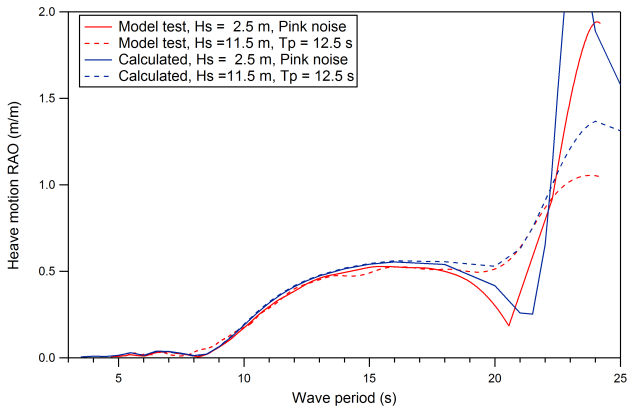

FIGURE 4. Heave motion response RAO without current.

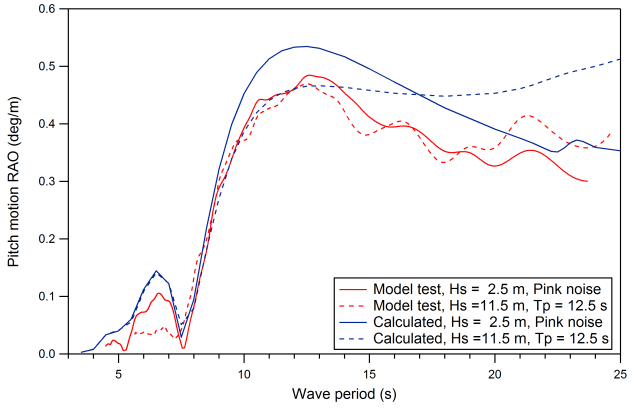

FIGURE 5. Pitch motion response RAO without current.

SURFACE ELEVATION AND AIR GAP

Free-surface elevation RAOs

The hydrodynamic boundary value problem is solved as an equivalent seakeeping problem with forward speed $-U$, where U is the current velocity in a rotated coordinate system with the

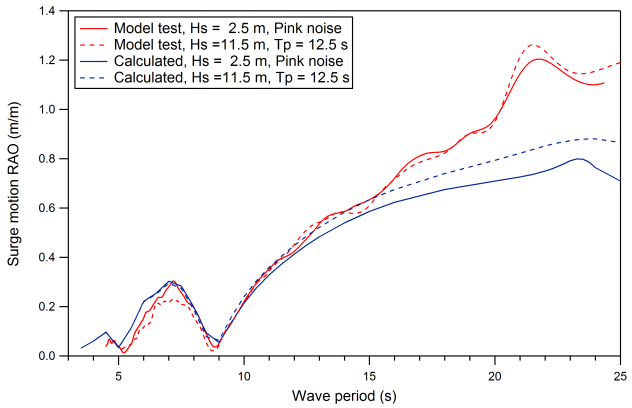

FIGURE 6. Surge motion response RAO with current speed 0.9 m/s.

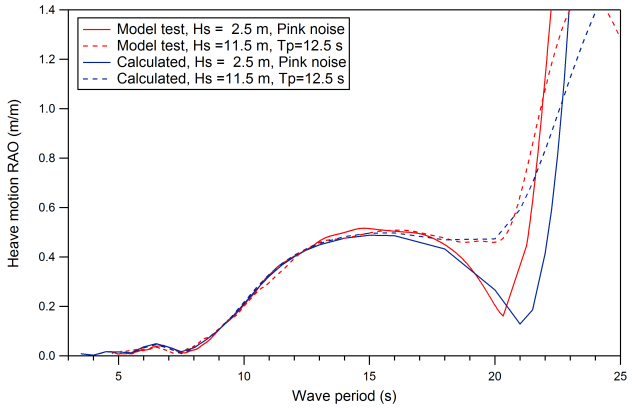

FIGURE 7. Heave motion response RAO with current speed 0.9 m/s.

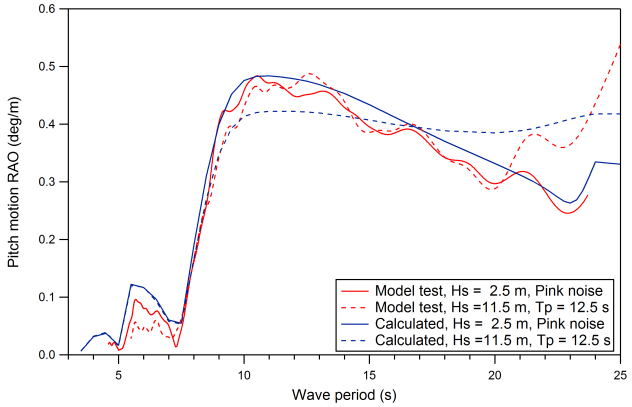

FIGURE 8. Pitch motion response RAO with current speed 0.9 m/s.

$x-$axis in the direction of the current. The total velocity potential in the fluid is then obtained as

$$\Phi = \bar{\phi} - Ux + \varphi \tag{1}$$

Here $\bar{\phi}$ is the steady disturbance potential for the double-body flow with free surface boundary condition $\bar{\phi}_z = 0$ on $z = 0$. φ_0 is the incident wave potential in the steady moving reference system and φ is the unsteady scattering and radiation potential. The free surface elevation is then obtained as

$$\zeta = -\frac{1}{g}\left(i\omega\varphi + (\bar{\phi}_x - U)\varphi_x + \bar{\phi}_y\varphi_y + \bar{\phi}_z\varphi_z\right) \tag{2}$$

Here ω is the encounter frequency which is related to the wave frequency ω_0 as

$$\omega = \omega_0(1 + \frac{\omega_0 U}{g}\cos\beta) \tag{3}$$

where β is the wave heading. $\beta = 0$ corresponds to waves along the positive $x-$axis. The unsteady first order velocity potential can be expressed as

$$\varphi = \left[\varphi_0 + \varphi_7 + \sum_{j=1}^{6}\varphi_j\eta_j\right]e^{i\omega t} \tag{4}$$

Here φ_7 is the scattering potential and φ_j is the radiation potential for mode of motion j. Further, η_j is the motion response amplitude for motion mode j at frequency ω.

The free surface elevation was not measured directly in the model tests, but it may be derived from the measured relative motion and the measured motion responses. The wave elevation both with and without current is calculated by MULDIF and shown in Figure 10. It is mainly included here for comparison with the relative motion given in Figures 11 and 12. The coordinates of the points where the free surface and relative motion are studied are listed in Table 1 and visualized in Figure 9.

Upwell RAOs

DNVGL's Offshore Technical Guidance DNVGL-OTG-13 [11] define the upwell χ as the relative motion between the water surface and the deck structure above as

$$\chi(x,y,t) = \eta(x,y,t) - z_p(x,y,t) \tag{5}$$

Here $z_p(x,y,t)$ is the vertical wave and wind induced motion of the unit at horizontal position (x,y) and $\eta(x,y,t)$ is the total surface elevation at the same horizontal position. Here, both z_p and η are defined as positive upwards. The upwell may further be decomposed as

$$\chi = \chi_{WF} + \chi_{LF} + \chi_{mean} \tag{6}$$

TABLE 1. Points on the free surface where the relative motion was measured in the Exwave semi model tests.

Position	x	y	Position	x	y
1	-47.10	0.00	2	-42.70	33.50
3	-46.70	33.50	4	-42.85	42.63

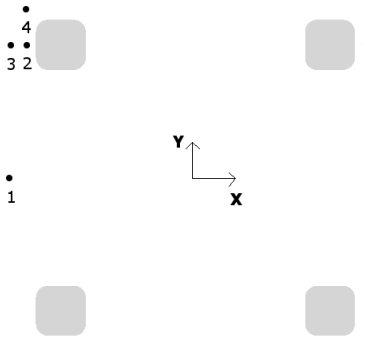

FIGURE 9. Points on the free surface where the relative motion was measured in the Exwave semi model tests. Zero degree wave heading indicates waves propagating along positive x-axis.

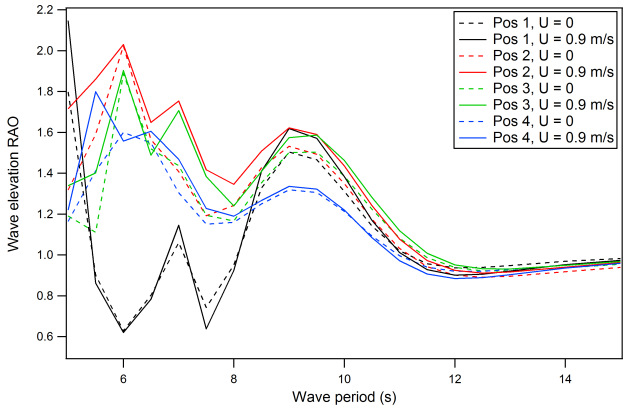

FIGURE 10. Calculated wave elevation RAO at the different positions. Wave heading 0 degrees, zero current and collinear current with speed 0.9 m/s.

where χ_{WF} is the wave-frequency contribution, χ_{LF} is the low-frequency contribution and χ_{mean} is the mean value due to a mean inclination of the floater. Determining the low-frequency contribution to the upwell requires that the mean vertical drift forces are calculated. At present, only calculation of mean horizontal drift forces is considered in MULDIF.

Airgap is defined as the distance between the bottom of the deck at horizontal position (x,y) and the wave surface

$$\begin{aligned} a(x,y,t) &= \left[a_0(x,y)+z_p(x,y,t)\right]-\eta(x,y,t) \\ &= a_0(x,y)-\chi(x,y,t) \end{aligned} \tag{7}$$

Deck impact will then occur if the airgap $a(x,y,t)<0$.

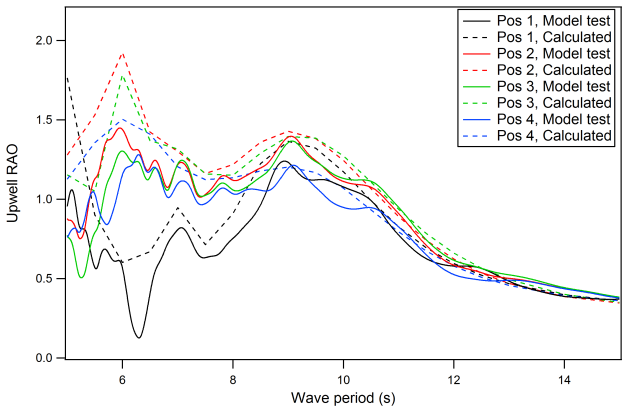

FIGURE 11. Calculated and measured upwell RAOs at the different positions. Wave heading 0 degrees, zero current.

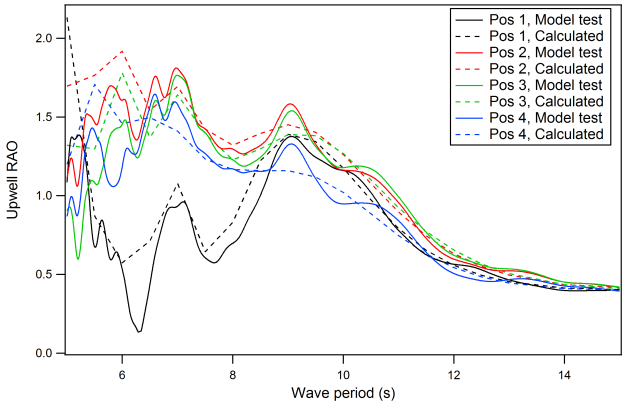

FIGURE 12. Calculated and measured upwell RAOs at the different positions. Wave heading 0 degrees, collinear current with speed 0.9 m/s.

Figures 11 and 12 present the calculated upwell RAOs plotted against the measured relative motion obtained by cross spectral analysis from the pink noise tests with $H_s = 2.5$m. The pink noise tests are performed with a spectrum with constant spectral value in the range $5-25$ s. The agreement is quite good, although some discrepancies can be seen for the lower periods.

The vertical motion z_p may generally be adequately predicted by a linear diffraction analysis, while the surface elevation $\eta(x,y,t)$ will in general include nonlinear effects and will thus represent a non-Gaussian process. By comparing the relative motion RAOs obtained from the pink noise tests ($H_s = 2.5$ m) with

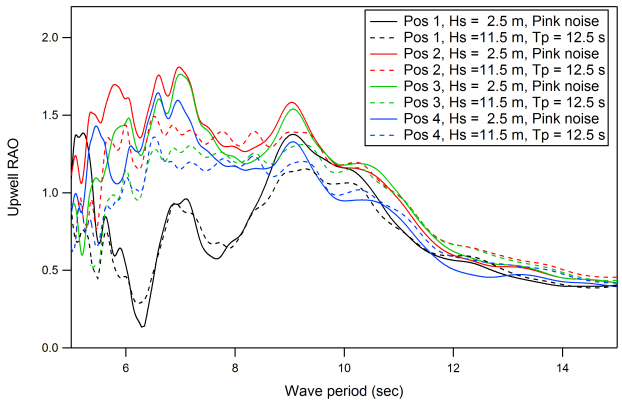

FIGURE 13. Measured upwell RAOs at the different positions. Wave heading 0 degrees, collinear current with speed 0.9 m/s. Obtained from two different sea states.

results obtained from the more severe sea state with $H_s = 11.5$ m and $T_p = 12.5$, the influence of non-linearities on the relative motion is seen to be significant, see Figure 13.

Numerical calculations

MULDIF can be used to visualize the effect of wave-current interaction effects. The wave amplification factor and upwell are presented as contour plots in Figures 14 and 15, respectively, including results both with and without wave-current interaction. Regular waves with wave period $T = 9$ s is considered, with waves and current propagating from left (heading 0 degrees). The coordinates of the panel vertices of the panels on the free surface are used as calculation points.

At this particular wave period, the wave-current interaction acts to increase the wave amplification factor in front of the semi, while less influence can be seen on the upwell. This can be explained by the motion of the semi, which is also influenced by the wave-current interaction. However, the surface elevation and upwell may vary significantly with the wave period, as shown in Hermundstad et.al. [1], and statistical analyzes will now be focused on.

Assuming that the wave frequency maxima of the upwell χ_{WF} follow a Rayleigh distribution, the extreme value distribution for the upwell in a sea state may be written as

$$F_\chi(x) = \left(1 - \exp\left(\frac{-x^2}{2\sigma_\chi^2}\right)\right)^N \tag{8}$$

where σ_χ^2 is the variance of the wave frequency upwell.

$$\sigma_\chi^2 = \int_0^\infty |\chi_{WF}|^2 S(\omega)\, d\omega \tag{9}$$

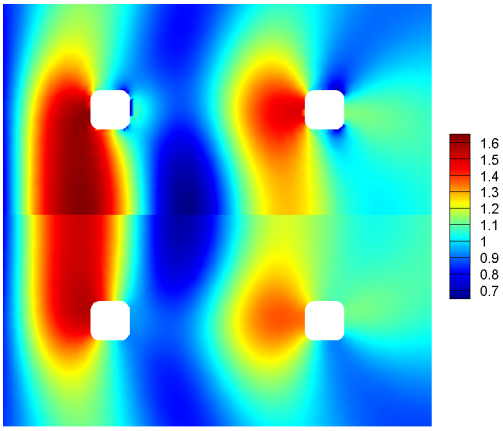

FIGURE 14. Wave amplification factor in regular waves with period $T = 9.0$ s and wave heading 0 degrees (propagating from left). Collinear current with speed 0.9 m/s in the upper half and zero current in the lower half.

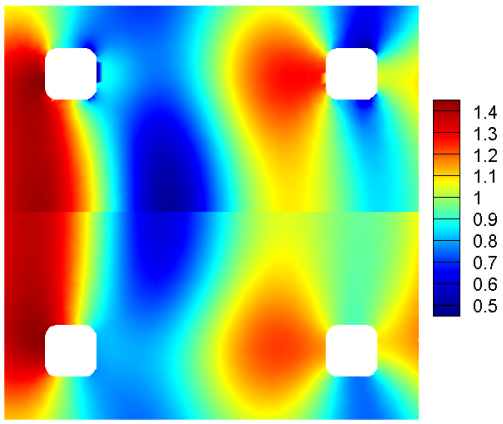

FIGURE 15. Upwell in regular waves with period $T = 9.0$ s and wave heading 0 degrees (propagating from left). Collinear current with speed 0.9 m/s in the upper half and zero current in the lower half.

N is the number of cycles of the wave frequency upwell in the duration D of the sea state which is usually taken as 3 hours.

$$N = \frac{D}{T_{z\chi}} \tag{10}$$

where $T_{z\chi}$ is the mean zero upcrossing period of the wave frequency upwell process.

$$T_{z\chi} = 2\pi\sqrt{\frac{m_{0\chi}}{m_{2\chi}}} \tag{11}$$

where the moments are given by

$$m_{n\chi} = \int_0^\infty |\chi_{WF}|^2 \, \omega^n S(\omega) \, d\omega \tag{12}$$

The upwell corresponding to a given annual probability q, χ_q can be taken as the 90% percentile level or $p = 0.90$ fractile in the extreme value distribution according to DNVGL-OTG-13 [11].

$$F_\chi(\chi_q) = p \tag{13}$$

or

$$\chi_q = \sigma_\chi \sqrt{-2\ln\left(1 - p^{1/N}\right)} \tag{14}$$

Further, the asymmetry factor α used to account for wave asymmetry and non-linear diffraction effects, can be determined as

$$\alpha = \frac{\eta_{90}}{\eta_{90}^{(L)}} \tag{15}$$

where the extreme value η_{90} is obtained from model tests assuming a Gumbel extreme value distribution, and $\eta_{90}^{(L)}$ is the extreme linear surface elevation obtained from a numerical analysis. The upwell can now be estimatied in a simplified manner at a distance not closer than 0.5D away from vertical columns with a characteristic diameter D.

$$\chi = \alpha \eta_{90}^{(L)} - z_p \tag{16}$$

The asymmetry factor is normally considered without current interaction. By applying MULDIF both with and without current, the effect of wave-current interaction on the asymmetry factor may be investigated. A correction factor accounting for the effect of current on the diffracted surface elevation is introduced as

$$\alpha_c = \frac{\eta_{90}^{(Lc)}}{\eta_{90}^{(L)}} \tag{17}$$

where $\eta_{90}^{(Lc)}$ is the extreme linear surface elevation obtained from a numerical analysis including wave-current interaction.

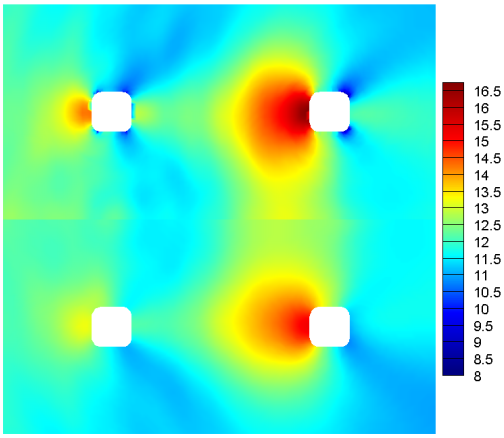

FIGURE 16. 90% percentile for the surface elevation with current speed 0.9 m/s in the upper half and zero current in the lower half. Torsethaugen (wind component) wave spectrum with $H_s = 11.5$ m and $T_p = 12.5$ s. Waves and current from left.

The 90% percentile for the surface elevation is plotted in Figure 16, including results both with and without current. Collinear waves and current propagating along the positive x-axis, i.e. from the left, are considered. The response values have been obtained using a Torsethaugen (wind component) wave spectrum with significant wave height $H_s = 11.5$ m and peak period $T_p = 12.5$ s with longcrested waves. In Figure 17 the correction factor α_c due to wave-current interaction is presented. It can be seen that the largest wave amplification factor is in front of the downstream columns, where also the effect of current is strongest.

A very brief screening of different wave and current directions shows that the surface elevation in irregular sea is increased by $10-12\%$ due to wave-current interaction for the current velocity of 0.9 m/s. This is significantly lower than the values referred to in the study by Zhang et.al [3]. In their study regular waves and various column diameters and spacings were investigated and current velocities up to 2.0 m/s were used. Their study concluded that the platform design may be an important factor in airgap considerations. The strong effects of the wave-current interaction obtained in regular waves will most probably be less pronounced in irregular sea.

To give an example of the influence of platform design on the wave-current interaction effect, the correction factor for the large production semi studied in Hermundstad et.al. [1] is presented in Figure 18. The same condition as presented in [1] is used. The current has a more pronounced effect on the surface elevation in front of the platform, and this is believed to be due to the large pontoons between the upstream columns.

The motion responses of the platform is also influenced by the wave-current interaction, and the 90% percentile for the upwell of the ExWave semi is plotted in Figure 19. A corresponding correction factor for the upwell is presented in Figure 20.

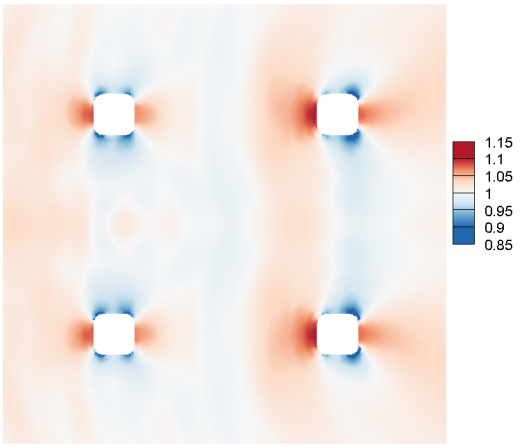

FIGURE 17. Correction factor for the surface elevation with current speed 0.9 m/s. Torsethaugen (wind component) wave spectrum with $H_s = 11.5$ m and $T_p = 12.5$ s. Waves and current from left.

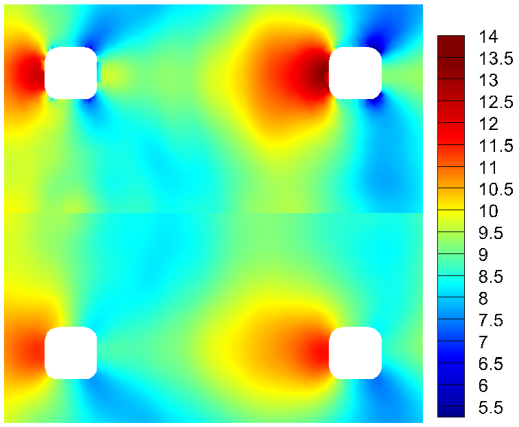

FIGURE 19. 90% percentile for the upwell with current speed 0.9 m/s in the upper half and zero current in the lower half. Torsethaugen (wind component) wave spectrum with $H_s = 11.5$ m and $T_p = 12.5$ s. Waves and current from left.

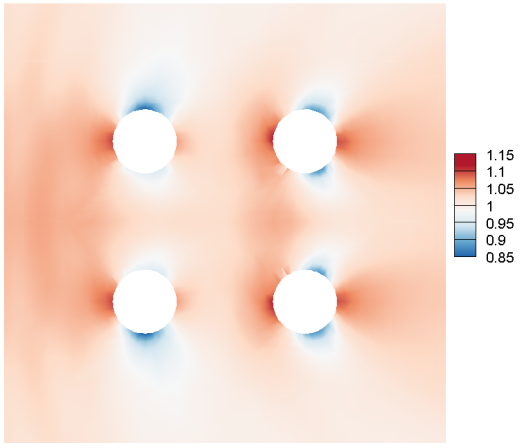

FIGURE 18. Correction factor for the surface elevation of a large production semi with current speed 1.2 m/s. Jonswap wave spectrum with $H_s = 14.5$ m and $T_p = 14.0$ s. Waves and current from left.

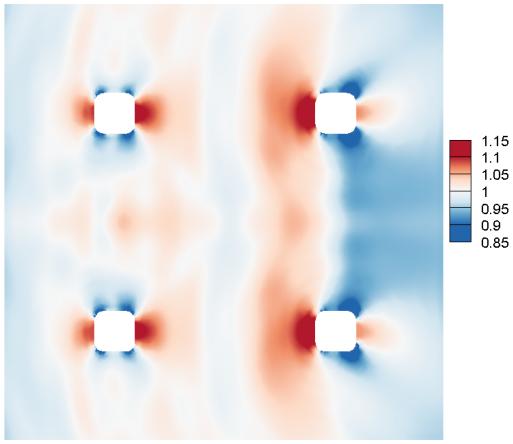

FIGURE 20. Correction factor for the upwell with current speed 0.9 m/s. Torsethaugen (wind component) wave spectrum with $H_s = 11.5$ m and $T_p = 12.5$ s. Waves and current from left.

Results for non-collinear waves and current are presented as the 90% percentiles for the upwell in waves with 45 degrees heading in Figure 21. The current direction is along the positive x-axis. Results without current are shown in Figure 22. The largest values of the upwell was found for this combination of wave and current direaction. The correction factors for surface elevation and upwell were however found to be of the same magnitude as the results in the collinear case.

Finally, Figures 23 and 24 show the 90% percentile for the surface elevation and upwell of the ExWave semi, respectively, obtained from the Torsethaugen wave spectrum with $H_s = 15.0$ m and $T_p = 16.0$ s. Corresponding correction factors for the surface elevation and upwell are presented in Figures 25 and 26. In this sea state it is seen that the wave-current interaction does not influence the surface elevation significantly, but it has effect on the motion response of the semi.

The discrepancies between calculated and measured upwell for low wave periods which can be seen in Figures 11 and 12, will not significantly influence the statistical results of the upwell for sea states of interest for airgap studies. The actual wave spectra will contain very little energy in this wave period range.

Small irregularities can be seen near the columns in the contour plots. These are due to numerical inaccuracies occurring at calculation points located very close to the columns. It can be avoided by moving the calculation points a small distance away from the columns.

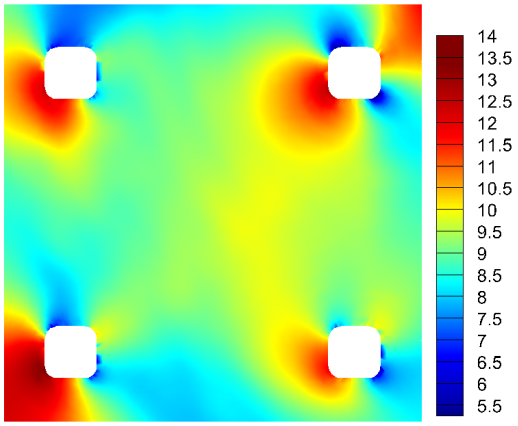

FIGURE 21. 90% percentile for the upwell with current speed 0.9 m/s. Torsethaugen (wind component) wave spectrum with $H_s = 11.5$ m and $T_p = 12.5$ s. Wave direction 45 degrees and current from left.

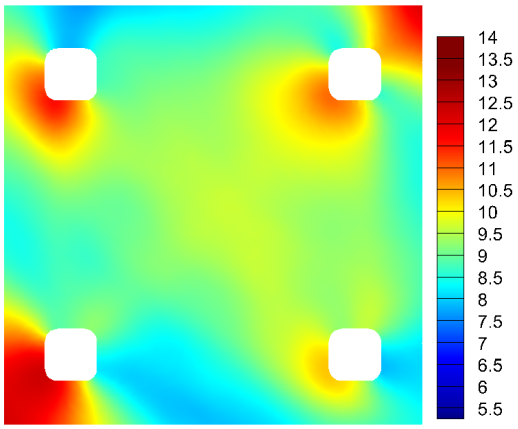

FIGURE 22. 90% percentile for the upwell without current. Torsethaugen (wind component) wave spectrum with $H_s = 11.5$ m and $T_p = 12.5$ s. Wave direction 45 degrees.

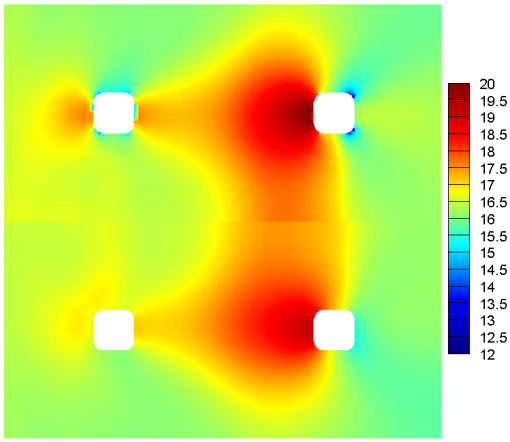

FIGURE 23. 90% percentile for the surface elevation with current speed 0.9 m/s in the upper half and zero current in the lower half. Torsethaugen (wind component) wave spectrum with $H_s = 15.0$ m and $T_p = 16.0$ s. Waves and current from left.

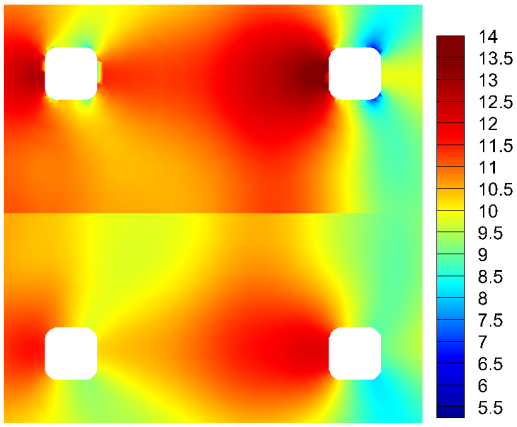

FIGURE 24. 90% percentile for the upwell with current speed 0.9 m/s in the upper half and zero current in the lower half. Torsethaugen (wind component) wave spectrum with $H_s = 15.0$ m and $T_p = 16.0$ s. Waves and current from left.

CONCLUSION

Calculations of motion response, surface elevation and upwell for semi-submersibles in waves and current have been carried out and compared with results from model tests. The initial validation against model test results show in general good agreement between numerical predictions and experimental results. For severe sea states it is important to include the contribution from the mooring system used in the model tests and viscous forces due to drag forces on bracings and pontoons. These forces are generally lower than the first order wave forces, but are important for wave periods close to the cancellation period where the first order wave forces are small.

A simple method to study the effect of wave-current interaction on upwell and thus airgap predictions is presented. The calculation of upwell is seen to have important contributions from wave-current interaction effects, both on the surface elevation and on the motion responses. These effects are expected to be more important with increasing current velocity.

ACKNOWLEDGMENT

This work has been carried out as a part of the MULDIF-2 JIP. Participants include: Statoil, Aker Solutions, National Oilwell Varco/APL, Rolls Royce Marine, DNV GL and SINTEF Ocean. The model test results for the ExWave semi-submersible were obtained as part of the ExWave JIP.

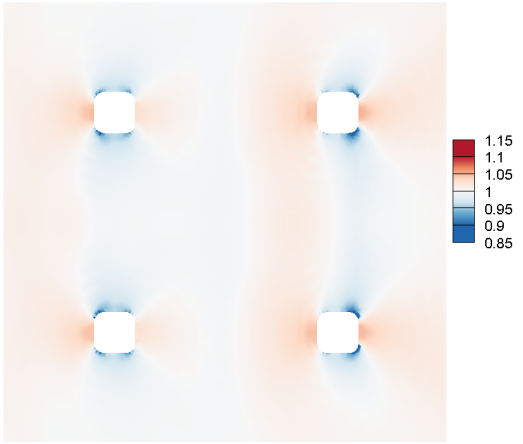

FIGURE 25. Correction factor for the surface elevation with current speed 0.9 m/s. Torsethaugen (wind component) wave spectrum with $H_s = 15.0$ m and $T_p = 16.0$ s. Waves and current from left.

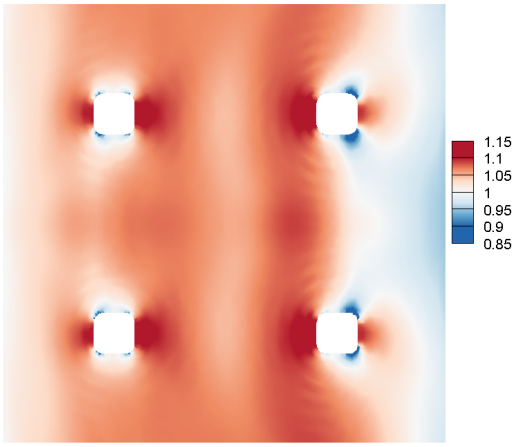

FIGURE 26. Correction factor for the upwell with current speed 0.9 m/s. Torsethaugen (wind component) wave spectrum with $H_s = 15.0$ m and $T_p = 16.0$ s. Waves and current from left.

REFERENCES

[1] Hermundstad, E. M., Hoff, J. R., Stansberg, C. T., and Baarholm, R. J., 2016. "Effects of wave-current interaction on floating bodies". In Proc. 35nd Int. Conf. Ocean, Offshore and Arctic Engineering, OMAE2016, June 19-24, Busan, South Korea.

[2] Zhiyuan, P., Vada, T., Finne, S., Nestegård, A., Hoff, J. R., Hermundstad, E. M., and Stansberg, C. T., 2016. "Benchmark study of numerical approahes for wave-current interaction problem of offshore floaters". In Proc. 35nd Int. Conf. Ocean, Offshore and Arctic Engineering, OMAE2016, June 19-24, Busan, South Korea.

[3] Zhang, F., Allers, J., and Xu, J., 2007. "Air-gap and wave run-up due to wave, current and body interaction". In Proc. 17th (2007) Int. Offshore and Polar Engng. Conf., Lisbon, Portugal.

[4] Zhao, R., Faltinsen, O., Krokstad, J. R., and Aanesland, V., 1988. "Wave-current interaction effects on large-volume structures". In Proc. 5th Intl. Conf. Behaviour of Offshore Struct. (BOSS'88), Trondheim, Norway, Vol. 2, pp. 623–638.

[5] Manuel, L., Sweetman, B., and Winterstein, S. R., 2001. "Analytical predictions of the air gap response of floating structures". *J. Offshore Mech. Arct. Eng,* ***123***(3), pp. 112–117.

[6] Stansberg, C. T., 2014. "Nonlinear wave amplification around column-based platforms in steep waves". In Proc. 33rd Int. Conf. Ocean, Offshore and Arctic Engineering, OMAE2014, June 8-1, San Francisco, California, USA.

[7] Sweetman, B., 2004. "Practical airgap prediction for offshore structures". *J. Offshore Mech. Arct. Eng,* ***126***(2), pp. 147–155.

[8] Sweetman, B., Winterstein, S. R., and Cornell, C. A., 2002. "Airgap analysis of floating structures: first- and second-order transfer functions from system identification". *Applied Ocean Research,* ***24***, pp. 107–118.

[9] Bratland, A. K., Haver, S., Stansberg, C. T., Zhang, F., Allers, J., Krokstad, J., and Ersdal, S., 2007. "A semi submersible in combined extreme waves and current – comparison of model tests and existing software". In Proc. of OMAE 2007, San Diego.

[10] Salvesen, N., Tuck, E. O., and Faltinsen, O., 1970. "Ship motions and sea loads". *SNAME Transactions,* ***78***, pp. 250–287.

[11] DNVGL-OTG-13, 2016. Prediction of air gap for column stabilised units. Tech. rep., DNV GL AS.